HHS Public Access

Author manuscript

Acta Biomater. Author manuscript; available in PMC 2020 May 01.

Published in final edited form as:

Acta Biomater. 2019 May ; 90: 205–216. doi:10.1016/j.actbio.2019.04.015.

Improving the adhesion, flexibility, and hemostatic efficacy of a sprayable polymer blend surgical sealant by incorporating silica particles

John L. Daristotle[a], **Shadden T. Zaki**[b], **Lung W. Lau**[c], **Leopoldo Torres Jr**[a], **Aristotelis Zografos**[b], **Priya Srinivasan**[c], **Omar B. Ayyub**[d], **Anthony D. Sandler**[c], and **Peter Kofinas**[d,*]

[a]Fischell Department of Bioengineering, University of Maryland, Room 3102 A. James Clark Hall, 8278 Paint Branch Dr., College Park, MD 20742, USA

[b]Department of Materials Science and Engineering, University of Maryland, 4418 Stadium Dr., College Park, MD 20742, USA

[c]Sheikh Zayed Institute for Pediatric Surgical Innovation, Joseph E. Robert Jr. Center for Surgical Care, Children's National Medical Center, 111 Michigan Avenue, NW Washington, DC 20010, USA

[d]Department of Chemical and Biomolecular Engineering, University of Maryland, 4418 Stadium Dr., College Park, MD 20742, USA

Abstract

Commercially available surgical sealants for internal use either lack sufficient adhesion or produce cytotoxicity. This work describes a surgical sealant based on a polymer blend of poly(lactic-co-glycolic acid) (PLGA) and poly(ethylene glycol) (PEG) that increases wet tissue adherence by incorporation of nano-to-microscale silica particles, without significantly affecting cell viability, biodegradation rate, or local inflammation. In functional studies, PLGA/PEG/silica composite sealants produce intestinal burst pressures that are comparable to cyanoacrylate glue (160 mmHg), ~2 times greater than the non-composite sealant (59 mmHg), and ~3 times greater than fibrin glue (49 mmHg). The addition of silica to PLGA/PEG is compatible with a sprayable in situ deposition method called solution blow spinning and decreases coagulation time in vitro and in vivo. These improvements are biocompatible and cause minimal additional inflammation, demonstrating the potential of a simple composite design to increase adhesion to wet tissue through physical, noncovalent mechanisms and enable use in procedures requiring simultaneous occlusion and hemostasis.

Keywords

Solution blow spinning; Surgical sealant; Tissue adhesive; Polymer composite fibers

*Corresponding author. kofinas@umd.edu (P. Kofinas).

Disclosures

The authors have no conflicts of interest.

Appendix A. Supplementary data

Supplementary data to this article can be found online at https://doi.org/10.1016/j.actbio.2019.04.015.

1. Introduction

Tissue sealing is necessary following many surgical procedures or traumatic injuries. Resections, biopsies, and accidental trauma may damage tissue and its vasculature and may require surgical reconstruction and hemostasis. Conventional wound closure devices like sutures are limited in their ability to seal some wounds due to tissue gaps, suture failure, or suture dehiscence [1,2]. In defined procedures such as bowel anastomosis, a leak occurs at a rate of 5–17% depending on patient characteristics [3,4]. Leaks can cause sepsis, a systemic infection with high morbidity and mortality rates and a challenging heath care issue for both diagnosis and treatment [5]. Similarly, achieving hemostasis remains an unavoidable challenge in tissue injury, especially for at-risk patients [6]. Surgical sealants supplement conventional wound closure devices by covering or filling the gaps of a closed wound with a layer of adhesive material [7]. Here, we investigate how incorporating silica particles of various sizes affects the wet tissue adhesion, flexibility, and hemostatic efficacy of a biodegradable polymer blend surgical sealant. These improvements are necessary to enable the surgical sealant to be used in procedures requiring simultaneous occlusion and coagulation. We also focus on the evaluating the biocompatibility of the composite sealants through cytotoxicity in vitro, as well as inflammation and immune response in a preliminary mouse model.

Surgical sealants are used in addition to sutures to repair or close tissues that are at risk for leak, infection, or blood loss. Common surgical sealants include fibrin glue and cyanoacrylate glue [8,9]. They are deposited as liquids, which makes them difficult to apply effectively because they can drip off vertical structures into adjacent tissue spaces. Additionally, water and protein present on the surface of internal tissues may prevent sufficient adhesion of these materials for internal applications [10]. Due to their limitations, commercially-available surgical sealants produce mixed results in clinical trials, sometimes failing to improve patient outcomes over conventional surgical techniques [11,12]. The field has largely focused on increasing tissue adhesion by forming covalent bonds with tissue proteins and curing materials in situ [13]. While fibrin glue can effectively form an enzymatically crosslinked network within itself and with tissue through specific reactions, synthetic surgical sealants often utilize highly reactive functional groups to achieve this—which can lead to increased cytotoxicity, swelling, and poor biodegradability [14,15]. In contrast, this work demonstrates an increase in tissue adhesion using nano-to-microscale silica particles. Incorporating silica particles into a synthetic polymer surgical sealant increases interfacial physical bonding to tissue and increases the energy dissipated by the bulk matrix, yielding greater burst pressure while producing no significant increase in cytotoxicity or local inflammation. For ease of use and accurate application, the surgical sealant can be spraydeposited as a conformal polymer fiber mat using solution blow spinning (SBS).

Poly(lactic-co-glycolic acid) (PLGA) and polyethylene glycol (PEG), a biodegradable and bioabsorbable polymer blend, can be spray-deposited as fibers using SBS yet transitions into a soft, conformal film after warming to body temperature [16,17]. Here, we suspended silica particles in PLGA/PEG blend solution that can be deposited in situ as composite fibers

directly onto wet soft tissues—which present a variety of hydrophilic surface chemistries that are challenging to adhere to [18]. Through a combination of nanotexture and crack suppression, the silica particles increase the flexibility, adhesion strength, and adhesion energy of the composite sealant. When exposed to blood, the silica particles induce coagulation that is complementary to the occlusion provided by the surgical sealant. We then validated the adhesive and hemostatic effects of the PLGA/PEG/silica composite sealant in an ex vivo model of intestinal anastomosis and an in vivo liver laceration model. The simple incorporation of silica particles produces no changes in cell viability or local inflammation, which was assessed in an in vivo intraperitoneal implantation model.

2. Materials and methods

2.1. Polymer deposition and polymer solution

An airbrush (Master Airbrush, G222-SET, 0.2 mm nozzle diameter) was used to deposit the surgical sealants [19]. The airbrush was connected to a compressed CO_2 tank equipped with a pressure regulator set to 20 psig. Unless stated otherwise, fiber mats were produced by solution blow spinning onto a 22 mm by 22 mm glass coverslip, with the distance between airbrush nozzle and cover slip at approximately 10 cm. For 500 mL of polymer solution, the spraying process typically produces 16 ± 5 mg of polymer fiber sample on the coverslip (n = 60). The typical thickness of the fiber mat is approximately 160 ± 30 mm for this solution volume and consistent across the sample [16]. All polymer solutions were dissolved in acetone, with 10% w/v PLGA (inherent viscosity = 0.86 dL g^{-1} in hexafluoroisopropanol, M_n = 48800 ± 500 g mol^{-1} measured with gel permeation chromatography against polystyrene standards, 50:50, Lactel), 5% w/v PEG (M_n = 950–1050 g mol^{-1} n, Sigma-Aldrich). 5% w/v silica particles were suspended in the PLGA/PEG solutions and dispersed by sonication. ~180 nm and ~620 nm silica particles were synthesized according to a Stöber process and washed with deionized water. 10–20 nm silica nanopowder was purchased from Sigma-Aldrich. Dynamic light scattering (DLS, Zetasizer Nano ZS90) was used to determine the hydrodynamic diameter of the Stöber particles.

2.2. Morphology characterization

Fiber samples were produced by solution blow spinning (SBS) 200 mL of polymer solution. For scanning electron microscopy (SEM, Hitachi SU-70), fiber samples on coverslips were sputter coated with gold before imaging. Fiber diameter was measured from SEM images in ImageJ (National Institutes of Health). Average fiber diameter was calculated for each sample using 2 different images, with 20 measurements made in each. When fibers were selected for measurement, nodes or intersections between fibers were not measured. Porosity was estimated using the DiameterJ plug-in for ImageJ (n = 12, 3 SEM images per group) [20]. Transmission electron microscopy (TEM) was performed on a JEOL 2100F using samples of fibers placed between two TEM grids.

2.3. Burst pressure testing

Porcine small intestine was purchased from a local butcher and cleaned with water prior to use. The small intestine was cut into 10 cm segments, and the ends were closed with zip ties for testing. A half diameter incision was made to simulate a leaky anastomosis. Tissue was

rehydrated and heated to 37 °C by soaking in 37 °C phosphate buffered saline (PBS) for two minutes, followed by exposure to 37 °C ambient air for four minutes, repeating this process twice, and finally drying with gauze (Fisherbrand). Approximately 500 mL of polymer solution was deposited directly onto the intestinal tissue using the SBS process described above. For cyanoacrylate and fibrin glue (Tisseel, Baxter), 500 mL of adhesive was applied. After applying the adhesive, it was allowed to set for 15 min at 37 °C in ambient air.

Once the adhesive was set, the intestine was connected to the burst pressure testing setup, which is diagrammed in Fig. 2A. A syringe was used to inject 1× phosphate buffered saline (PBS) dyed with 0.05% methylene blue [notdef] into the intestine at a constant rate using an 18 gauge needle. A digital pressure gauge was attached to the injection line using a three-way stopcock to measure the injection pressure. The maximum pressure prior to bursting or leakage was recorded as the burst pressure. The entire test was captured on video so that the failure mode could be determined. Each adhesive was tested five times ($n = 5$).

2.4. Interfacial imaging

Samples of porcine small intestine were rehydrated and heated to 37 °C using the same procedure as samples for burst pressure testing, but during the last rehydration step, PBS was replaced with a solution of 33% glycerol in PBS to preserve the samples during freezing. 500 mL of polymer solution was deposited directly onto a sample of small intestine. The samples were submerged in liquid nitrogen and fractured to produce a cross-section of the interface between intestinal tissue and surgical sealant. SEM (Hitachi SU-70) was used to image the samples, which were sputter-coated with gold before imaging.

2.5. Differential scanning calorimetry (DSC)

Fiber samples were produced by solution blow spinning (SBS) 500 mL of polymer solution. The resulting fiber mats were removed from the coverslips and trimmed to yield 10 mg samples of fibers. The samples were then sealed in aluminum hermetic pans (TA Instruments) using a sample encapsulation press. DSC measurements were made on a TA Instruments DSC Q100. Samples were held isothermal at −50 °C for 5 min and then heated and cooled from −50 to 80 to −50 °C, at a rate of 3 °C min^{-1}, ±0.20 °C amplitude, with a modulation period of 60 s for two continuous cycles. T_g onset was calculated using the tangent intersection method on the reversing heat flow. The inflection point of the reversing heat flow during the T_g was used to determine the midpoint.

2.6. Tensile testing

Fiber samples were produced by solution blow spinning (SBS) 500 mL of polymer solution. The resulting fiber mats were removed from the coverslips and trimmed to a rectangular shape, approximately 10 mm by 5 mm in size. Exact sample dimensions were measured immediately prior to testing. Tensile tests were made using a TA Instruments DMA Q800 equipped with a film tension clamp. Samples were stretched under a controlled force ramp from 0 N to 5 N at a rate of 0.001 N/min. Measurements were made either at room temperature or at 37 °C after a 10 min isothermal period. Elastic modulus was calculated from the linear region of the resulting stress/strain curve. Each sample type was replicated 5 times ($n = 5$).

2.7. Pull-off adhesion testing

Fiber samples were produced by solution blow spinning (SBS) 2 mL of polymer solution. The resulting fiber mats were removed from the coverslips and folded into 5 mm by 5 mm samples that weighed approximately 50 mg. Thickness was measured for each sample prior to testing, and averaged 0.9 ± 0.1 mm across all fiber samples. For fibrin glue, samples with similar size and mass were created by depositing approximately 50 mL of Tisseel (Baxter International Inc., Deerfield IL). Pull-off testing was performed on the TA Instruments DMA Q800. Before testing the samples, each 1 cm clamp was coated with 50 mL of 20 mg Ml^{-1} Type 1 Collagen (rat tail) solution (Sigma-Aldrich). The sample was compressed at 0.001 N for 30 min at 37 °C before testing to allow for a complete thermal transition to occur. After compressing at 1 N for 1 min, a controlled force ramp was used to increase pull-off force at a rate of 1 N min^{-1} until failure, also at 37 °C. Failure type was recorded as either adhesive or cohesive. Each sample type was replicated five times ($n = 5$).

2.8. Wound closure adhesion testing

Wound closure adhesion testing was performed on the TA Instruments DMA Q800. 1 cm by 1 cm sections of porcine small intestine were attached to rectangular clamps using cyanoacrylate glue. Small intestine was warmed in ambient air to 37 °C before testing. The rectangular clamps were brought together end to end, and 1 mL of sealant polymer solution, 50 mL of cyanoacrylate glue, or 50 mL of fibrin glue (Tisseel, Baxter International Inc., Deerfield IL) was deposited on this joint, closing the gap between the two intestine-coated clamps (see ASTM F2458–05) [21]. The sealant was carefully applied and trimmed to avoid coating the interface between the ends and edges of the clamps. It was then allowed to set at 37 °C for 10 min before testing. A controlled force ramp was used to increase force at a rate of 1 N min^{-1} until failure. Failure type was recorded as either adhesive or cohesive. Force values were normalized to the surface area of intestine coated by the adhesive, which was measured using calipers, giving adhesive strength. Each sample type was replicated five times ($n = 5$).

2.9. Cell viability

Cell viability was assessed in vitro with L929 mouse fibroblasts (ATCC #CCL-1) using a WST-1 assay. L929s were cultured in media consisting of Dulbecco's minimum essential medium supplemented with 10% fetal bovine serum, 1% streptomycin and 1% glutamine. Cells were plated at 10^4 cells per well in 100 mL of media in a 96 well plate and incubated at 37C and 5% CO_2 for 24 h. The culture media was then replaced with sealant extract samples. Stock extracts from sealant samples were prepared by immersing 50 mg of fiber mat sample in 500 mL of the culture media at 37 °C for 24 h. Fiber mat samples were produced by solution blow spinning (SBS) 2 mL of polymer solution onto a sterile 22 mm by 22 mm glass coverslip. The resulting fiber mats were removed from the glass coverslips and folded into samples that weighed approximately 50 mg. Cells were then cultured in 100 mL dilutions of the stock extract at 37 °C for 24 h: 1×dilution (100% stock extract), 10×dilution (10% stock extract Media in fresh media), and 100×dilution (1% stock extract media in fresh media). The control media was not exposed to a surgical sealant sample. The positive control was puromycin at 25 mg mL^{-1} in culture media. Viability was measured at

24 h using an WST-1 assay (Roche). Absorbance was measured at 480 nm using a Synergy-H4 plate reader (BioTek). This experiment was repeated 4 times for each extract ($n = 4$).

2.10. Degradation

Samples of polymer blend surgical sealant were prepared on glass coverslips by solution blow spinning 2 mL of polymer solution. A microbalance (Sartorius ME-5) was used to determine the net increase in mass after the spinning process was complete, which is the initial sample mass, m_i. Samples were placed in 6 well plates, submerged in 4 mL of 1 PBS, and stored in a shaker incubator at 37°C and 50 rpm. PBS was exchanged every 48 h for 28 days to prevent pH change. Samples were removed at time points of 0, 1, 3, 7, 14, and 28 days. At these points, the PBS was removed, and the samples were stored in a vacuum desiccator for three days. The samples were weighed again to determine the final mass, m_f, and mass loss ($m_i - m_f$) was calculated as a percentage of m_i. Samples that swell with water may produce a negative mass loss because of incomplete water removal and salt that remains in the polymer matrix. Five samples were used for each time point and surgical sealant type ($n = 5$).

2.11. Coagulation time

Citrated whole sheep blood was warmed to 37 °C. First, 1 mL of whole blood was added and mixed in a glass vial containing 10 mg of polymer blend surgical sealant samples, which were collected from fiber mats blow spun onto glass coverslips. Immediately after this step, the blood was recalcified using a 0.2 M $CaCl_2$ stock, yielding a final $CaCl_2$ concentration in blood of 10 mM. Coagulation was assessed by vial inversion, as previously described [22,23]. Coagulation time was defined as when the entire sample was stagnant during inversion. A Lab-quake rotator was used to invert the vials continuously while they were being examined for complete coagulation. Control trials received no surgical sealant. The experiment was repeated 5 times ($n = 5$) for each type of surgical sealant.

2.12. Hemostatic testing in porcine liver laceration

All animal procedures were approved by the Children's National Medical Center Institutional Animal Care And Use Committee (IACUC protocol #00030454), and the animals were treated in accordance with PHS Policy on Humane Care and Use of laboratory Animals, the National Institute of Health Guide for the Care and Use of Laboratory Animals, and the Animal Welfare Act. A 15 kg female Yorkshire swine (Archer Farms, MD, USA) was used. After intubation and sedation per standard protocol, a midline laparotomy was made. Four 2 cm lacerations and two wedge resections were separately made on the liver (total of 6 wounds, n = 3 per group). Sealant was applied immediately after wound creation. Liver wounds were assessed for bleeding after application of sealant. Surgical sealant was removed to assess the degree of hemostasis at the liver wounds after 10 min.

2.13. Intraperitoneal space implantation model

All animal procedures were approved by the Children's National Medical Center Institutional Animal Care And Use Committee (IACUC protocol #00030703), and the animals were treated in accordance with PHS Policy on Humane Care and Use of laboratory

Animals, the National Institute of Health Guide for the Care and Use of Laboratory Animals, and the Animal Welfare Act. Eighteen, 7–15 week-old C57BL/6 female mice were used (Jackson Laboratory, ME). Mice were randomized into three groups based on type of implant: control (saline injection), PLGA/PEG, and P-620 implants. Experimental endpoints were 3 days and 10 days from initial surgery. A total of three mice were allocated to each treatment group per endpoint. Surgical sealant implants were made under sterile conditions by solution blow spinning 2 mL of polymer solution onto a sterile cover slip then cutting the resulting fiber mat into 5 mm disks weighing approximately 10 mg using a sterile skin biopsy punch (Acuderm, FL) in a biosafety cabinet. After processing, the implants were sterilized by UV irradiation.

All mice were anesthetized with a solution of ketamine and xylazine. Buprenorphine was given for analgesic at the start of the surgery and then every 12 h for 48 h. After anesthesia, the mice were positioned supine, abdominal hair removed, and then skin prepped with betadine solution. In sterile fashion, a 1 cm laparotomy incision was made at the midline. After dissection into the peritoneal cavity, the 5 mm diameter surgical sealant disks were implanted into the right lower quadrant. For the saline injection control, 0.2 mL of sterile saline was dripped into the right lower quadrant. Animals were sacrificed 3 or 10 days after initial surgery. After euthanasia, cardiac puncture was performed for serum cytokine assessment. Midline laparotomy was also performed, and images of the peritoneal cavity were taken with a 15-megapixel digital camera (Canon, USA). The intraperitoneal space was then examined by a surgeon for signs of inflammation.

2.14. Histological analysis and disk diameter

Surgical sealant implants along with surrounding tissue were retrieved from the intraperitoneal space for analysis. The sealant disks were measured after retrieval, and the change in size was calculated as a fraction of the original 5 mm diameter. Then, surgical sealant and surrounding tissue were prepared for histology by paraffin fixation. 5 lm sections were stained with hematoxylin and eosin.

2.15. Serum inflammatory cytokine analysis

Whole blood was collected via sterile syringe and 25-gauge needle. In sterile, uncoated vials, blood was allowed to clot over 15 min, then serum extracted from supernatant after centrifugation for 15 min at 4 °C and 2000 RPM. Serum was stored at−80 °C until ELISA analysis for INFγ and TNFα. Analysis was performed using ELISA kits (Mouse TNFa High Sensitivity ELISA and Mouse INFγ Platinum ELISA, Invitrogen, NY) on serum samples in duplicate. Serum concentrations were interpolated from standard curves.

2.16. Statistical analysis

A one-way ANOVA was used to analyze variance between groups in studies with more than two experimental groups, followed by Tukey’s multiple comparisons test with a = 0.05 to determine between which two groups there was a significant difference. All error bars are equal to the standard error. Statistical analysis was performed in Origin 8.

3. Results

3.1. Solution blow spinning of polymer-silica composite fibers

Composite fiber sealants were deposited in situ by solution blow spinning polymer-particle mixtures in acetone from an airbrush. Silica particles were suspended in a polymer solution of 10% w/v PLGA and 5% w/v PEG dissolved in acetone. Particles were suspended at a concentration of 5% w/v and formed an opaque but homogenous mixture (Fig. S1A)–a unique property of silica, which has high colloidal stability in acetone [24]. Particles added in concentrations greater than 5% suspended inconsistently and soon after mixing produced aggregates that settled.

Silica particles were used to study the effect of particle size on adhesion primarily because they can be synthesized in monodisperse size distributions, allowing the effect of particle size to be isolated. We utilized the Stöber process to synthesize spherical particles with monodisperse hydrodynamic diameter distributions of 180 nm and 620 nm, as measured by dynamic light scattering (DLS) [25]. Silica nanopowder with size range of 10–20 nm, which is used in FDA-approved pharmaceutical applications, was also tested. Together, these groups of particles span a size range from approximately 10 nm to 1 mm (Table 1). Combinations of 10% w/v PLGA, 5% w/v PEG, and 5% w/v particles in acetone were studied to determine the effect of particle size on adhesion to tissue, fiber morphology, and mechanical properties. The corresponding weight fractions, volume fractions, and specific surface area of the particles in the solid is provided in Table 2. Blends containing particles are denoted “P-X,” where X is the average particle diameter.

Increasing particle size increased the diameter of fibers produced. Fiber morphology changed from relatively thin, long, and bundled fibers when 20 nm particles were used to thick, branching fiber webs with 620 nm particles (Fig. 1A–D). Fiber diameters were greater when particles of greater diameter were used (Fig. 1E). Using a portable airbrush, the SBS process allows for direct deposition onto a target organ for surgical sealing and hemostasis (Fig. 2A). The porosity of all fiber mats averaged 49 ± 7%, with no significant differences between any two spinning solutions used.

3.2. Tissue adhesion of composite sealants depends on silica particle size

Tissue adhesion was assessed in a representative ex vivo model, by performing burst pressure testing on sealed segments of porcine intestinal tissue (Fig. S3). Particle-polymer composite sealants produced greater burst pressures than the non-composite control (Fig. 2B). P-620, the composite fiber sealants containing the largest nanoparticles tested, resulted in a burst pressure of 160 ± 30 mmHg, approximately double the burst pressure recorded for PLGA/PEG sealants containing no nanoparticles (59 ± 3 mmHg, $p = 0.007$) and fibrin glue (49 ± 8 mmHg, $p = 0.002$), a clinical control. P620’s average burst pressure was similar to those observed with cyanoacrylate glue (171 ± 6 mmHg), which is the most tissue adherent sealant amongst clinical controls. Intermediate particle sizes also resulted in increases in burst pressure relative to the control. Approaches to chemically modify the surface of the particles with polydopamine functional groups did not increase burst pressure (Figs. S1B and S2).

Samples of intestinal tissue were sealed ex vivo at 37 °C, cryopreserved, and freeze-fractured to create a cross-sectional image of the interface between tissue and sealant. This provided imaging of the particles in P−620 that can interact with PLGA polymer chains and proteins from both sides of the interface. While PLGA fiber mats have minimal surface contact due to their fibrous morphology (Fig. 2C) PLGA/PEG becomes a film that evenly coats the tissue (Fig. 2D). Unlike either PLGA or PLGA/PEG, P−620 forms a tight interface with tissue and has micro-scale texture, as described above (Fig. 2E). Despite transitioning to a conformal film, many micron-sized regions of P−620 show the ability to bond to tissue simultaneously, instead of behaving as one film with a flat interface. The interface of P−620 with tissue has little to no void space (Fig. 2E inset, blue arrows) even when compared to PLGA and PLGA/PEG, which despite being conformal have gaps in tissue coverage (Fig. 2C inset and Fig. 2D inset, orange arrows).

3.3. Thermal and mechanical properties are affected by silica particle size

We expected that differences in thermal and mechanical properties of the sealants contributed to the differences in burst pressure that we observed between different composite sealants. Toughness, stiffness, extensibility, and transition temperature affect the sealant's ability to form a conformal fiber mat during deposition, transition rapidly into an adherent film, and change in shape as the intestine expands with fluid. A sealant will ideally exhibit low stiffness, high toughness, and high extensibility, such that it can be deformed without restricting the natural change in the intestine's shape under physiological forces, while the transition temperature will occur above room temperature but below body temperature (37 °C) to allow for the deposition of fibers that set to become a coherent film during surgery.

At 31 °C, the semi-crystalline PEG in blow spun PLGA/PEG fibers melts, yielding a morphological change from fibers to a soft, homogenous film. At body temperature, fibers sprayed directly onto tissue transition to a conformal film, increasing surface coverage and eliminating large voids adjacent to the interface. Prior to the fiber to film transition, the spherical particles in the composite sealants are distributed throughout the fibers (transmission electron microscopy, Fig. 3A) and can create surface roughness roughly proportional to the radius of the particles (Fig. 3B).

The temperature-dependent morphological transition of PLGA/PEG is characterized by an endotherm at 31 °C corresponding to the melting of PEG on its first heating cycle, after which the sealant shows a single glass transition temperature (T_g) indicating homogenization of the blend and miscibility of PLGA and PEG (Fig. 4A). Modulated differential scanning calorimetry (MDSC) was used to scan the composite fiber mats for this behavior, with no premelt cycle. The melting endotherm of PEG is observed in all polymer composites, but T_m is slightly depressed. 20 nm silica particles increased the T_g of P-20, while P−620's T_g was unaffected (Fig. S4). Silica particles also increase the amount of time it takes for the sealant to transition when heated in 37 °C air (Table S1).

It has recently been demonstrated that increased toughness, elasticity, and extensibility improve surgical sealant performance [27,28]. Tensile mechanical testing was conducted at room temperature (Fig. S5A) and body temperature (37 °C, Fig. S5B) on a DMA Q800 (TA

Instruments). Depending on the size of the particles used in the composite sealants, stiffness and failure strain could be increased or decreased (Fig. 4B–C). The smaller particles in P-20 produced stiffer materials that failed at lower strains, consistent with the increased T_g observed in MDSC analysis. Incorporating larger particles produced the opposite effect: P-620 had significantly lower modulus and greater failure strain.

The larger particles in P−620 suppress its brittle failure, increasing its failure strain compared to PLGA/PEG. This is consistent with the toughening mechanisms proposed in the literature for polymer-particle composites [29]. Stress is concentrated on the particles, suppressing crack formation and creating small regions of high strain where debonding of the polymer matrix from particles may occur [30]. Toughness (Fig. 4D) and ultimate tensile strength (Fig. 4E) are similar for all samples, indicating that the composite sealants were not compromised by the high loading of silica particles. In wound closure strength testing (Fig. S6), which is primarily influenced by the cohesive strength of the adhesive, the stiffer P−20 produces higher values. In general, polymers reinforced with rigid particles display reduced strength but increased toughness, due to suppressed crack propagation [31].

3.4. Adhesion energy and strength increase for composite sealants

Pull-off testing was performed at 37 °C on the DMA Q800 using collagen-coated compression clamps (Fig. 5A). Because the bulk of P−620 can be deformed to higher strains at lower force, the adhesive can dissipate energy through plastic deformation before adhesive failure (Fig. 5A, inset and Fig. 5B). The combination of low stiffness and high failure strain directly translates to approximately 20 times greater adhesion energy (Fig. 5C). 4 of 5 PLGA/PEG samples failed at the interface, indicating that the bulk material's cohesive strength exceeds the strength of adhesive bonding, while none of the P−620 samples failed at the interface. Switching the failure mode from adhesive to cohesive is a critical feature of P −620 enabled simply by incorporating silica particles. This property was not present in P−20 because surface-area dependent confinement effects increase the T_g of the PLGA/PEG matrix, making its extensibility lower than PLGA/PEG. Pull-off adhesion force was also significantly enhanced by the silica particles, increasing by 25% (Fig. 5A). P-620's force and energy were significantly greater than fibrin glue ($p < 0.0001$). Interfacial adhesion and bulk toughening mechanisms are illustrated in Fig. 5D, which shows the adsorption of molecules from both surfaces to the particles and the local regions of high deformation near the particles that allow for greater deformation.

3.5. Assessing biocompatibility of composite surgical sealants

The controlled release of silica particles from the PLGA matrix limits their cytotoxicity compared to the administration of colloidal suspensions of these particles, which has been thoroughly investigated in the literature for silica particles of many sizes and types. Amorphous silica's cytotoxicity to murine epidermal cells is around 100 μg/mL when dispersed in cell culture media, but with a strong dependence on particle size: larger particles produce lower cytotoxicity, likely because they have different, slower cell uptake mechanisms [32]. Amorphous silica particles also have known accumulation and excretion patterns [33]. After 24 h of exposure to extractions from blow spun fiber mats of P−20, P −180, and P-620, cell viability is only slightly limited when compared to PLGA and

PLGA/PEG (Fig. 6A). This suggests that particles are eluted slowly into the media and that they contribute minimal cytotoxicity. Prior investigations of solution blow spinning biodegradable polymer fibers from acetone show that acetone has no negative effect on cell viability [16,19].

To verify that degradation of the sealants occurs complementary to the timeline for adequate wound healing and is not affected by particulate components, a study of mass loss during degradation was conducted by incubating fiber mats in PBS at 37 °C. PLGA/PEG fiber mats typically maintain mechanical integrity for about 28 days, allowing for support throughout the wound healing process, but lose a substantial amount of mass in the first few days as highly water-soluble PEG is released from the polymer matrix (Figs. 6B and S7, mass spectrometry). The tested particle composite fiber mats showed a similar degradation profile. After the initial burst release of PEG, there is a slow, constant release of material from the solid polymer matrix.

3.6. Silica decreases coagulation time and improves hemostasis in vivo

Achieving hemostasis is critical to avoiding surgical complications. We preliminarily assessed the hemostatic effects of PLGA/PEG composite fiber mats using a clotting time test (Fig. 6C). PLGA/PEG fiber mats inhibit clot formation, likely due to the high amount of PEG composing the fibers, which can interfere with critical enzymatic reactions in the coagulation cascade. Silica, which has a high negative surface charge and is a known hemostat due to the glass effect [34], decreases the clotting time compared to PLGA/PEG in all cases. P−620 returns clotting time to control levels, while P−20 significantly decreases clotting time by approximately 25% compared to the control. These results show that incorporating silica into PLGA/PEG has additional utility in promoting hemostasis, which will allow the composite sealants to be used in surgical procedures with high amounts of potential blood loss.

To simulate the use of PLGA/PEG and P-620 as hemostats in vivo, we sprayed the sealants directly onto a bleeding porcine liver immediately after resection (Video S1 and Video S2). This approach models a procedure such as liver resection, which has increased morbidity due to the risk of significant blood loss [35]. Immediately after deposition, PLGA/PEG showed blood permeating the sealant (Fig. 6D) while P−620 maintained a seal (Fig. 6E). When the sealants were removed after 10 min (Video S3 and Video S4), the surface of the liver coated with PLGA/PEG had not achieved hemostasis (Fig. 6F), while the surface coated with P−620 had stopped bleeding except for a large vessel (Fig. 6G), which is indicated by the green arrow. Incorporating silica improves the hemostatic efficacy of the PLGA/PEG polymer blend.

3.7. Composite sealants produce minimal additional inflammation

To further demonstrate the biocompatibility of the PLGA-silica composite surgical sealants, we assessed biodegradation and the potential immune response in a mouse intraperitoneal implantation model. Composite sealants were implanted to determine if incorporating silica within a polymer matrix affects biodegradation, local inflammation, or systemic immune response. PLGA/PEG and P-620 sealant samples were fabricated into 5 mm diameter disks

that were implanted into the right lower quadrant of the abdomen. After implantation, the implanted sealant disk became attached to the abdominal fat pads (5 of 6 PLGA/PEG implants, 6 of 6 P-620 implants). There was no gross inflammation observed, and the peritoneum appeared normal, similar to that of the control group that received a saline injection (Fig. 7A). After 3 days, the sealant was engulfed within the fat pads (Fig. 7B and C). Despite swelling moderately at 3 days, the size of the sealant disks ultimately decreased over the duration of the 10-day implantation (Fig. 7D), matching well with the mass loss rate in vitro (Fig. 6B). All mice survived to the experimental endpoints without any signs of illness or distress.

Recent studies have shown that biomaterials implanted in the intraperitoneal space adhere to the abdominal fat pads, where they can be fibrosed and create the potential for an immune response[36]. Therefore, we measured the serum levels of two cytokines, tumor necrosis factor alpha (TNFα) and interferon gamma (INFγ), that are increased during acute inflammation and macrophage activation. Despite increasing slightly, there were no significant differences in TNFα levels over time or between PLGA/PEG and P620 (Fig. 7E), indicating that there was minimal systemic inflammation. INFγ levels increased significantly at day 10 for P-620 (Fig. 7F), indicating that the silica particles may have caused macrophage activation, but serum levels of IFNγ are still low compared to levels for an acute inflammatory response, which can be higher than 100 pg mL^{-1} [37]. While the abdominal fat pads generally show minimal collagen content, a thin layer of fibrosis and inflammatory cell infiltration (black arrow) was observed at the interface with the surgical sealant (blue arrow) for both PLGA/PEG and P-620 after 3 days (Fig. 7G). After 10 days, there is additional collagen deposition and cell infiltration throughout the surgical sealant (Fig. 7H). Ongoing fibrosis at the interface of P-620 with the fat pad corroborates the increased 10-day INFγ serum levels.

Based on these results, incorporating silica into PLGA-PEG creates a more persistent local inflammatory response. However, the lack of overt signs of inflammation in the intraperitoneal cavity, such as erythema, edema, and adhesion development, indicate that the level of acute inflammation is small for both sealants and localized to just the tissue-sealant interface. Overall, PLGA/PEG and P-620 produce minimal additional acute inflammation in the intraperitoneal space, where they are expected to be used.

4. Discussion

Surgical sealants are typically deposited as viscous fluids and form crosslinked matrices after curing. Fibrin glue, which has excellent biocompatibility, achieves this by enzymatic crosslinking of a biologically-derived precursor solution. However, synthetic approaches to increase adhesion based on crosslinking and covalent bonding to tissue may exacerbate cytotoxicity or inflammation by exposing the surgical site to reactive functional groups [38]. Misapplication of flowable sealant precursors due to poor ease of use creates the potential for large sealant droplets to be deposited into the vasculature, which leads commercially available surgical sealants such as fibrin glue to be contraindicated for application into highly vascularized tissue or onto heavy arterial or venous bleeding. PLGA/PEG/silica surgical sealants invert this paradigm, depositing an initially stiff matrix of composite fibers

that soften and become adhesive upon heating to body temperature. Unlike a curable surgical sealant, PLGA/PEG/silica adheres only to the site where the solid fiber mat is initially sprayed.

The polymer-particle composite design incorporates both micro and nanoscale structures that increase the adhesive force. This can be attributed to particles at the interface increasing interfacial bonding energy [39–41]. However, these principles have only been applied to improving hydrogel adhesion to tissue [42]. The approach investigated in the current work alternatively uses SBS to fabricate a solid adhesive polymer matrix with embedded particles. Just as silica microparticles in P−620 suppress crack formation in the bulk, enhancing its extensibility (Fig. 4C) and adhesion energy, the microparticles can also suppress cracks at the interface, creating a stronger adhesive bond (Fig. 5A). Crack suppression has been shown to improve interfacial adhesion by increasing fracture energy in hydrogel-based systems [43,44].

Despite the turbulent nature of the SBS process, incorporating particles into the blow spinning solution creates sealants with a consistent nanoscale texture that is visible on the surface of fibers, as shown in Fig. 2E and Fig. 3A–B. Using silica produces composite fibers with much higher loading of particles compared to previous research on blow spun composites [45]. Such surface nanoarchitectures have been discovered to contribute significantly to the adhesive footpads of small animals, such as the gecko [46]. This knowledge then inspired the design of micropatterned adhesive materials [47]. But, the majority of adhesive nanostructured polymer surfaces in the literature have been fabricated using etched or patterned templates and 3D direct laser writing [48,49]. Fabricating the adhesive sealant using SBS yields conformal materials with site-specific sizing adaptable to any tissue defect, an advantage over prefabricated nanostructured adhesives.

This simple composite approach yields a solid, biodegradable, and fully synthetic surgical sealant with enhanced adhesion in burst pressure (Fig. 2B) and pull-off adhesion (Fig. 5A) tests. Swelling is much lower than in synthetic hydrogel sealants such as Coseal (Fig. 7D), similar to low-swelling or negative-swelling tissue adhesives [15,50]. Burst pressure in our ex *vivo* model is significantly greater than the clinical standard, fibrin glue, and comparable to cyanoacrylate (Fig. 2B). P-620, at 160 ± 30 mmHg, produces in vitro burst pressures comparable to dual-network tissue adhesives [43] (roughly 200 mmHg) and photopolymerized gelatin sealants [51] (~100 mmHg) in similar models on *ex vivo* tissue. Interestingly, PLGA/PEG/silica sealants at body temperature (E ~1–10 kPa, Fig. 4B) have a lower Young's modulus than other tissue adhesives, which typically have E > 25 kPa [52]. This allows them to be deformed and move with the soft tissues being sealed. Tuning of silica particle size can produce increased flexibility, due to crack suppression by larger, micron-sized particles (Fig. 4B), or faster blood coagulation (Fig. 6C) when using 20 nm silica.

Silica particles decrease coagulation time of PLGA/PEG, a critical feature that allows PLGA/PEG/silica composites to be deployed for hemostasis (Fig. 6D–H). For nuisance bleeding and other surgical procedures where noncovalent polymer adhesion and occlusion would be sufficient, it could be used instead of delivering prohemostatic coagulation factors.

Silica particles trigger hemostasis through their high surface charge and physical adsorption [34,53]. The combination of occlusion and hemostasis provided by PLGA/PEG/silica is an alternative to modern biologically derived or recombinant hemostats, which deliver fibrinogen supplemented with combinations of thrombin and/or Factor XIII to specifically target exposed extracellular matrix and create or crosslink a fibrin clot [54,55]. Synthetic polymers that bind fibrin are also capable of targeting a wound site in this manner to promote hemostasis [56].

PLGA/PEG/silica produces low levels of inflammation, only slightly increasing macrophage activation (Fig. 7F) and cell infiltration (Fig. 7G–H) without producing any difference in gross inflammation of the IP space (Fig. 7A–C). Immune response may occur in extended degradation studies. For use as a surgical sealant, long-term studies in large animal models are necessary to demonstrate a reduction in the observed complication rate associated with soft tissue wound closure, either due to prevention of blood loss or leak. While the purpose of a surgical sealant is to occlude, for use in the clinic it must demonstrate efficacy in reducing complication rate, a holistic metric that encompasses leakage, abscess formation, other adverse events that may cause a re-operation, septic shock, or death [57].

5. Conclusions

The present work demonstrates that PLGA/PEG/silica composite surgical sealants offer increased adhesion, burst pressure, and hemostasis compared to pure polymer blend sealants. Other properties, such as stiffness, failure strain, and T_g are affected by particle size. 620 nm silica particles provide a number of advantages over other particle sizes and the non-composite control, maximizing burst pressure. Ultimately, the incorporation of silica particles into PLGA/PEG increased tissue adhesion by providing a nanostructured contact area and increasing energy dissipation. These benefits are the result of enhanced interfacial interactions facilitated by the particles, a change in adhesive failure mode from adhesive to cohesive failure, and composite toughening mechanisms, especially crack suppression. Biodegradation, cytotoxicity, and inflammation are minimally affected by the incorporation of particles, and these sealants are deliverable directly to the site of surgery as fiber mats using solution blow spinning.

Supplementary Material

Refer to Web version on PubMed Central for supplementary material.

Acknowledgements

We acknowledge the support of the Maryland NanoCenter, the AIMLab, the Functional Macromolecular Laboratory, and the Sheikh Zayed Institute for Pediatric Surgical Innovation.

Funding sources

Research reported in this publication was supported by the National Institute of Biomedical Imaging and Bioengineering of the National Institutes of Health under Award Number R01EB019963. J.L.D. was supported by the National Institute of Biomedical Imaging and Bioengineering of the National Institutes of Health under Award Number F31EB025735. The content is solely the responsibility of the authors and does not necessarily represent the official views of the National Institutes of Health. This material is based upon work supported by the National

Science Foundation Graduate Research Fellowship Program (L.T. Jr.) under Grant No. DGE1322106. S.T.Z and T.Z. received support from the University of Maryland ASPIRE program.

References

[1]. Schäfer K, Loeweneck H, Stanka H, Ernst R, Zumtobel V, Disorders of microcirculation in colon anastomoses and their significance for the pathogenesis of suture dehiscence, Langenbecks Arch. Chir. 375 (1989) 24–32, 10.1007/BF00186117.

[2]. Annabi N, Tamayol A, Shin SR, Ghaemmaghami AM, Peppas NA, Khademhosseini A, Surgical materials: Current challenges and nano-enabled solutions, Nano Today 9 (2014) 574–589, 10.1016/j.nantod.2014.09.006. [PubMed: 25530795]

[3]. Hammond J, Lim S, Wan Y, Gao X, Patkar A, The burden of gastrointestinal anastomotic leaks: an evaluation of clinical and economic outcomes, J. Gastrointest. Surg. 18 (2014) 1176–1185, 10.1007/s11605-014-2506-4. [PubMed: 24671472]

[4]. Chittmittrapap S, Spitz L, Kiely EM, Brereton RJ, Anastomotic leakage following surgery for esophageal atresia, J. Pediatr. Surg. 27 (1992) 29–32. [PubMed: 1552439]

[5]. Rhee C, Dantes R, Epstein L, Murphy DJ, Seymour CW, Iwashyna TJ, Kadri SS, Angus DC, Danner RL, Fiore AE, Jernigan JA, Martin GS, Septimus E, Warren DK, Karcz A, Chan C, Menchaca JT, Wang R, Gruber S, Klompas M, for the CDC prevention epicenter program, incidence and trends of sepsis in US hospitals using clinical vs claims data, 2009–2014, JAMA (2017), 10.1001/jama.2017.13836.

[6]. Behrens AM, Sikorski MJ, Kofinas P, Hemostatic strategies for traumatic and surgical bleeding: hemostatic strategies for traumatic and surgical bleeding, J. Biomed. Mater. Res. Part A 102 (2014) 4182–4194, 10.1002/jbm.a.35052.

[7]. Annabi N, Yue K, Tamayol A, Khademhosseini A, Elastic sealants for surgical applications, Eur. J. Pharm. Biopharm. 95 (2015) 27–39, 10.1016/j.ejpb.2015.05.022. [PubMed: 26079524]

[8]. Kheirabadi BS, Field-Ridley A, Pearson R, MacPhee M, Drohan W, Tuthill D, Comparative study of the efficacy of the common topical hemostatic agents with fibrin sealant in a rabbit aortic anastomosis model, J. Surg. Res. 106 (2002) 99–107, 10.1006/jsre.2002.6426. [PubMed: 12127814]

[9]. Ensari CO, Genc V, Cakmak A, Erkek B, Karayalcin K, Effects of N-butyl-2-cyanoacrylate on high-level jejunojejunostomy, Eur. Surg. Res. 44 (2010) 13–16, 10.1159/000257969. [PubMed: 19907184]

[10]. Lang N, Pereira MJ, Lee Y, Friehs I, Vasilyev NV, Feins EN, Ablasser K, O'Cearbhaill ED, Xu C, Fabozzo A, Padera R, Wasserman S, Freudenthal F, Ferreira LS, Langer R, Karp JM, del Nido PJ, A blood-resistant surgical glue for minimally invasive repair of vessels and heart defects, Sci. Transl. Med 6 (2014) 218ra6, 10.1126/scitranslmed.3006557.

[11]. van der Ham AC, Kort WJ, Weijma IM, van den Ingh HF, Jeekel J, Effect of fibrin sealant on the healing colonic anastomosis in the rat, Br. J. Surg. 78 (1991) 49–53. [PubMed: 1998864]

[12]. Houston KA, Rotstein OD, Fibrin sealant in high-risk colonic anastomoses, Arch. Surg. 123 (1988) 230–234, 10.1001/archsurg.1988.01400260118015. [PubMed: 2449148]

[13]. Bouten PJM, Zonjee M, Bender J, Yauw STK, van Goor H, van Hest JCM, Hoogenboom R, The chemistry of tissue adhesive materials, Prog. Polym. Sci. 39 (2014) 1375–1405, 10.1016/j.progpolymsci.2014.02.001.

[14]. Mizrahi B, Stefanescu CF, Yang C, Lawlor MW, Ko D, Langer R, Kohane DS, Elasticity and safety of alkoxyethyl cyanoacrylate tissue adhesives, Acta Biomater. 7 (2011) 3150–3157, 10.1016/j.actbio.2011.04.022. [PubMed: 21569875]

[15]. Henise J, Hearn BR, Santi DV, Kamata H, Sakai T, Ashley GW, Surgical sealants with tunable swelling, burst pressures, and biodegradation rates, J. Biomed. Mater. Res. B Appl. Biomater. 105 (2016) 1602–1611, 10.1002/jbm.b.33701. [PubMed: 27149244]

[16]. Behrens AM, Lee NG, Casey BJ, Srinivasan P, Sikorski MJ, Daristotle JL, Sandler AD, Kofinas P, Biodegradable-polymer-blend-based surgical sealant with body-temperature-mediated adhesion, Adv. Mater. 27 (2015) 8056–8061, 10.1002/adma.201503691. [PubMed: 26554545]

[17]. Kern NG, Behrens AM, Srinivasan P, Rossi CT, Daristotle JL, Kofinas P, Sandler AD, Solution blow spun polymer: a novel preclinical surgical sealant for bowel anastomoses, J. Pediatr. Surg. (2016), 10.1016/j.jpedsurg.2016.11.044.

[18]. Artzi N, Zeiger A, Boehning F, Bon Ramos A, Van Vliet K, Edelman ER, Tuning adhesion failure strength for tissue-specific applications, Acta Biomater. 7 (2011) 67–74, 10.1016/j.actbio.2010.07.008. [PubMed: 20624496]

[19]. Behrens AM, Casey BJ, Sikorski MJ, Wu KL, Tutak W, Sandler AD, Kofinas P, In situ deposition of PLGA nanofibers via solution blow spinning, ACS Macro Lett. 3 (2014) 249–254, 10.1021/mz500049x.

[20]. Hotaling NA, Bharti K, Kriel H, Simon CG, DiameterJ: A validated open source nanofiber diameter measurement tool, Biomaterials 61 (2015) 327–338, 10.1016/j.biomaterials.2015.05.015. [PubMed: 26043061]

[21]. Sealants (2015).

[22]. Behrens AM, Sikorski MJ, Li T, Wu ZJ, Griffith BP, Kofinas P, Blood aggregating hydrogel particles for use as a hemostatic agent, Acta Biomaterialia. 10 (2014) 701–708, 10.1016/j.actbio.2013.10.029. [PubMed: 24185001]

[23]. Scola MR, Baggesen LM, Nichols TC, Key NS, Gallippi CM, A review of current methods for assessing hemostasis in vivo and introduction to a potential alternative approach, Thromb. Res. 129 (2012) S57–S61, 10.1016/j.thromres.2012.02.035. [PubMed: 22405050]

[24]. Ketelson HA, Pelton R, Brook MA, Colloidal stability of Stöber silica in acetone, Langmuir 12 (1996) 1134–1140.

[25]. Stöber W, Fink A, Bohn E, Controlled growth of monodisperse silica spheres in the micron size range, J. Colloid Interface Sci. 26 (1968) 62–69.

[26]. Sahu D, Kannan GM, Tailang M, Vijayaraghavan R, In vitro cytotoxicity of nanoparticles: a comparison between particle size and cell type, J. Nanosci. 2016 (2016) 1–9, 10.1155/2016/4023852.

[27]. Assmann A, Vegh A, Ghasemi-Rad M, Bagherifard S, Cheng G, Sani ES, Ruiz-Esparza GU, Noshadi I, Lassaletta AD, Gangadharan S, Tamayol A, Khademhosseini A, Annabi N, A highly adhesive and naturally derived sealant, Biomaterials 140 (2017) 115–127, 10.1016/j.biomaterials.2017.06.004. [PubMed: 28646685]

[28]. Annabi N, Rana D, Shirzaeiani E, Portillo-Lara R, Gifford JL, Fares MM, Mithieux SM, Weiss AS, Engineering a sprayable and elastic hydrogel adhesive with antimicrobial properties for wound healing, Biomaterials 139 (2017) 229–243, 10.1016/j.biomaterials.2017.05.011. [PubMed: 28579065]

[29]. Johnsen BB, Kinloch AJ, Mohammed RD, Taylor AC, Sprenger S, Toughening mechanisms of nanoparticle-modified epoxy polymers, Polymer 48 (2007) 530–541, 10.1016/j.polymer.2006.11.038.

[30]. Argon AS, Cohen RE, Toughenability of polymers, Polymer 44 (2003) 6013–6032, 10.1016/S0032-3861(03)00546-9.

[31]. Jordan J, Jacob KI, Tannenbaum R, Sharaf MA, Jasiuk I, Experimental trends in polymer nanocomposites—a review, Mater. Sci. Eng., A 393 (2005) 1–11, 10.1016/j.msea.2004.09.044.

[32]. Kim I-Y, Joachim E, Choi H, Kim K, Toxicity of silica nanoparticles depends on size, dose, and cell type, Nanomed. Nanotechnol. Biol. Med. 11 (2015) 1407–1416, 10.1016/j.nano.2015.03.004.

[33]. Fu C, Liu T, Li L, Liu H, Chen D, Tang F, The absorption, distribution, excretion and toxicity of mesoporous silica nanoparticles in mice following different exposure routes, Biomaterials 34 (2013) 2565–2575, 10.1016/j.biomaterials.2012.12.043. [PubMed: 23332175]

[34]. Ostomel TA, Shi Q, Stoimenov PK, Stucky GD, Metal oxide surface charge mediated hemostasis, Langmuir 23 (2007) 11233–11238, 10.1021/la701281t. [PubMed: 17892311]

[35]. Manas DM, Figueras J, Azoulay D, Garcia Valdecasas JC, French J, Dixon E,O'Rourke N, Grovale N, Mazzaferro V, Expert opinion on advanced techniques for hemostasis in liver surgery, Eur. J. Surg. Oncol. 42 (2016) 1597–1607, 10.1016/j.ejso.2016.05.008. [PubMed: 27329369]

[36]. Doloff JC, Veiseh O, Vegas AJ, Tam HH, Farah S, Ma M, Li J, Bader A, Chiu A, Sadraei A, Aresta-Dasilva S, Griffin M, Jhunjhunwala S, Webber M, Siebert S, Tang K, Chen M, Langan E,

Dholokia N, Thakrar R, Qi M, Oberholzer J, Greiner DL, Langer R, Anderson DG, Colony stimulating factor-1 receptor is a central component of the foreign body response to biomaterial implants in rodents and non-human primates, Nat. Mater. 16 (2017) 671, 10.1038/nmat4866. [PubMed: 28319612]

[37]. Mottas I, Bekdemir A, Cereghetti A, Spagnuolo L, Yang Y-SS, Müller M, Irvine DJ, Stellacci F, Bourquin C, Amphiphilic nanoparticle delivery enhances the anticancer efficacy of a TLR7 ligand via local immune activation, Biomaterials 190–191 (2019) 111–120, 10.1016/j.biomaterials.2018.10.031.

[38]. Spotnitz WD, Burks S, Hemostats, sealants, and adhesives: components of the surgical toolbox, Transfusion 48 (2008) 1502–1516, 10.1111/j.1537-2995.2008.01703.x. [PubMed: 18422855]

[39]. Rose S, Prevoteau A, Elzière P, Hourdet D, Marcellan A, Leibler L, Nanoparticle solutions as adhesives for gels and biological tissues, Nature 505 (2013) 382–385, 10.1038/nature12806. [PubMed: 24336207]

[40]. Baït N, Grassl B, Derail C, Benaboura A, Hydrogel nanocomposites as pressure-sensitive adhesives for skin-contact applications, Soft Matter 7 (2011) 2025, 10.1039/c0sm01123a.

[41]. Okada M, Nakai A, Hara ES, Taguchi T, Nakano T, Matsumoto T, Biocompatible nanostructured solid adhesives for biological soft tissues, Acta Biomater. 57 (2017) 404–413, 10.1016/j.actbio.2017.05.014. [PubMed: 28483692]

[42]. Pandey N, Hakamivala A, Xu C, Hariharan P, Radionov B, Huang Z, Liao J, Tang L, Zimmern P, Nguyen KT, Hong Y, Biodegradable nanoparticles enhanced adhesiveness of mussel-like hydrogels at tissue interface, Adv. Healthc. Mater. (2017) 1701069, 10.1002/adhm.201701069.

[43]. Yuk H, Zhang T, Lin S, Parada GA, Zhao X, Tough bonding of hydrogels to diverse non-porous surfaces, Nat. Mater. 15 (2016) 190–196, 10.1038/nmat4463. [PubMed: 26552058]

[44]. Li J, Celiz AD, Yang J, Yang Q, Wamala I, Whyte W, Seo BR, Vasilyev NV, Vlassak JJ, Suo Z, Mooney DJ, Tough adhesives for diverse wet surfaces, Science 357 (2017) 378–381. [PubMed: 28751604]

[45]. Vural M, Behrens AM, Hwang W, Ayoub JJ, Chasser D, Cresce A. von W, Briber RM, Kofinas P, Spray-processed composites with high conductivity and elasticity, ACS Appl. Mater. Interfaces 10 (2018), 10.1021/acsami.8b00068.

[46]. Huber G, Mantz H, Spolenak R, Mecke K, Jacobs K, Gorb SN, Arzt E, Evidence for capillarity contributions to gecko adhesion from single spatula nanomechanical measurements, PNAS 102 (2005) 16293–16296, 10.1073/pnas.0506328102. [PubMed: 16260737]

[47]. Geim AK, Dubonos SV, Grigorieva IV, Novoselov KS, Zhukov AA, Shapoval SY, Microfabricated adhesive mimicking gecko foot-hair, Nat. Mater. 2 (2003) 461–463, 10.1038/nmat917. [PubMed: 12776092]

[48]. Greiner C, Arzt E, del Campo A, Hierarchical gecko-like adhesives, Adv. Mater. 21 (2009) 479–482, 10.1002/adma.200801548.

[49]. Röhrig M, Thiel M, Worgull M, Hölscher H, 3D direct laser writing of nano- and microstructured hierarchical gecko-mimicking surfaces, Small 8 (2012) 3009–3015, 10.1002/smll.201200308. [PubMed: 22778085]

[50]. Barrett DG, Bushnell GG, Messersmith PB, Mechanically robust, negative- swelling, mussel-inspired tissue adhesives, Adv. Healthc. Mater. 2 (2013) 745–755, 10.1002/adhm.201200316. [PubMed: 23184616]

[51]. Vuocolo T, Haddad R, Edwards GA, Lyons RE, Liyou NE, Werkmeister JA, Ramshaw JAM, Elvin CM, A Highly elastic and adhesive gelatin tissue sealant for gastrointestinal surgery and colon anastomosis, J. Gastrointest. Surg. 16 (2012) 744–752, 10.1007/s11605-011-1771-8. [PubMed: 22081305]

[52]. Vakalopoulos KA, Wu Z, Kroese L, Kleinrensink G-J, Jeekel J, Vendamme R,Dodou D, Lange JF, Mechanical strength and rheological properties of tissue adhesives with regard to colorectal anastomosis: an ex vivo study, Ann. Surg. 261 (2015) 323–331, 10.1097/SLA.0000000000000599. [PubMed: 24670843]

[53]. Pourshahrestani S, Kadri NA, Zeimaran E, Towler MR, Well-ordered mesoporous silica and bioactive glasses: promise for improved hemostasis, Biomater. Sci. 7 (2019) 31–50, 10.1039/C8BM01041B.

[54]. Calcaterra J, Van Cott KE, Butler SP, Gil GC, Germano M, van Veen HA, Nelson K, Forsberg EJ, Carlson MA, Velander WH, Recombinant human fibrinogen that produces thick fibrin fibers with increased wound adhesion and clot density, Biomacromolecules 14 (2013) 169–178, 10.1021/bm301579p. [PubMed: 23215461]

[55]. Carlson MA, Calcaterra J, Johanning JM, Pipinos II, Cordes CM, Velander WH, A totally recombinant human fibrin sealant, J. Surg. Res. 187 (2014) 334–342, 10.1016/j.jss.2013.09.039. [PubMed: 24169144]

[56]. Chan LW, Wang X, Wei H, Pozzo LD, White NJ, Pun SH, A synthetic fibrin cross-linking polymer for modulating clot properties and inducing hemostasis, Sci. Transl. Med. 7 (2015). 277ra29–277ra29.

[57]. Silecchia G, Boru CE, Mouiel J, Rossi M, Anselmino M, Morino M, Toppino M, Gaspari A, Gentileschi P, Tacchino R, Basso N, The use of fibrin sealant to prevent major complications following laparoscopic gastric bypass: results of a multicenter, randomized trial, Surg. Endosc. 22 (2008) 2492–2497, 10.1007/s00464-008-9885-0. [PubMed: 18365278]

Statement of Significance

Incorporating silica particles increases the tissue adhesion of a polymer blend surgical sealant. The particles enable interfacial physical bonding with tissue and enhance the flexibility of the bulk of the sealant, without significantly affecting cytotoxicity, inflammation, or biodegradation. These studies also demonstrate how silica particles decrease blood coagulation time.

This surgical sealant improves upon conventional devices because it can be easily deposited with accuracy directly onto the surgical site as a solid polymer fiber mat. The deposition method, solution blow spinning, allows for high loading in the composite fibers, which are sprayed from a polymer blend solution containing suspended silica particles. These findings could easily be translated to other implantable or wearable devices due to the versatility of silica particles.

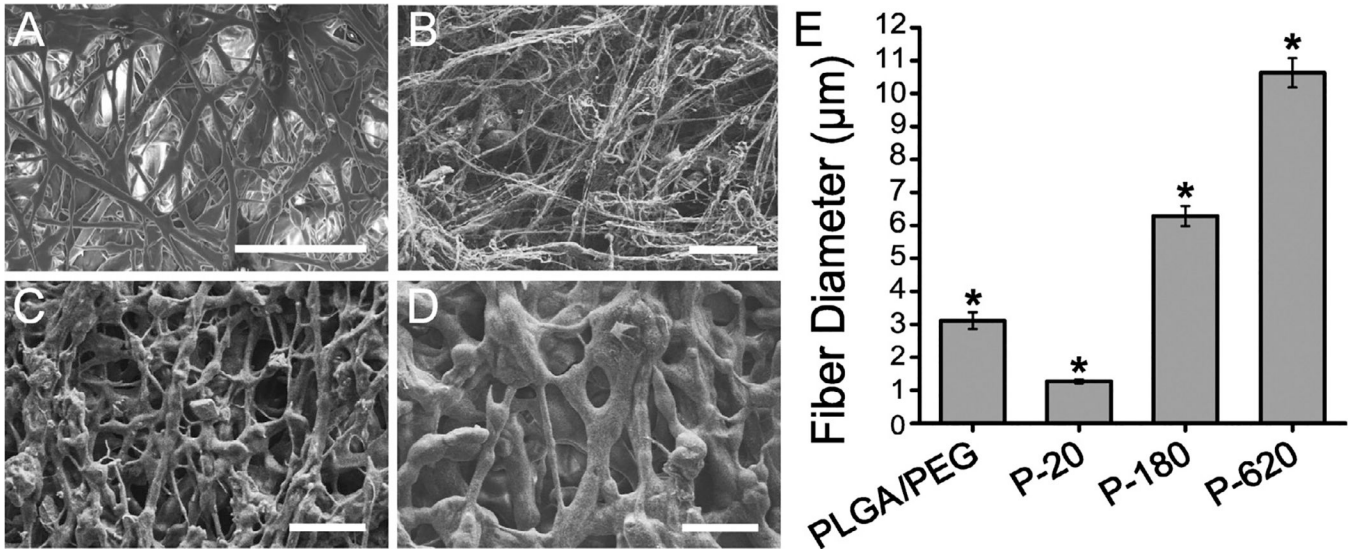

Fig. 1.

Particle size can increase or decrease the fiber diameter produced by solution blow spinning suspensions of silica particles in a polymer blend solution. Scanning electron microscope (SEM) images of fiber mats sprayed from (A) PLGA/PEG: 10% w/v PLGA, 5% w/v PEG solution in acetone (B) P-20: 10% w/v PLGA, 5% PEG, 5% 20 nm silica nanoparticles, (C) P-180: 10% w/v PLGA, 5% PEG, 5% 180 nm silica nanoparticles, and (D) P-620: 10% w/v PLGA, 5% PEG, 5% 620 nm silica nanoparticles. Scale bars = 50 mm. (E) Average fiber diameter measured from 20 fibers in 3 images using ImageJ. Asterisk indicates statistically significant difference ($p < 0.01$) between the groups.

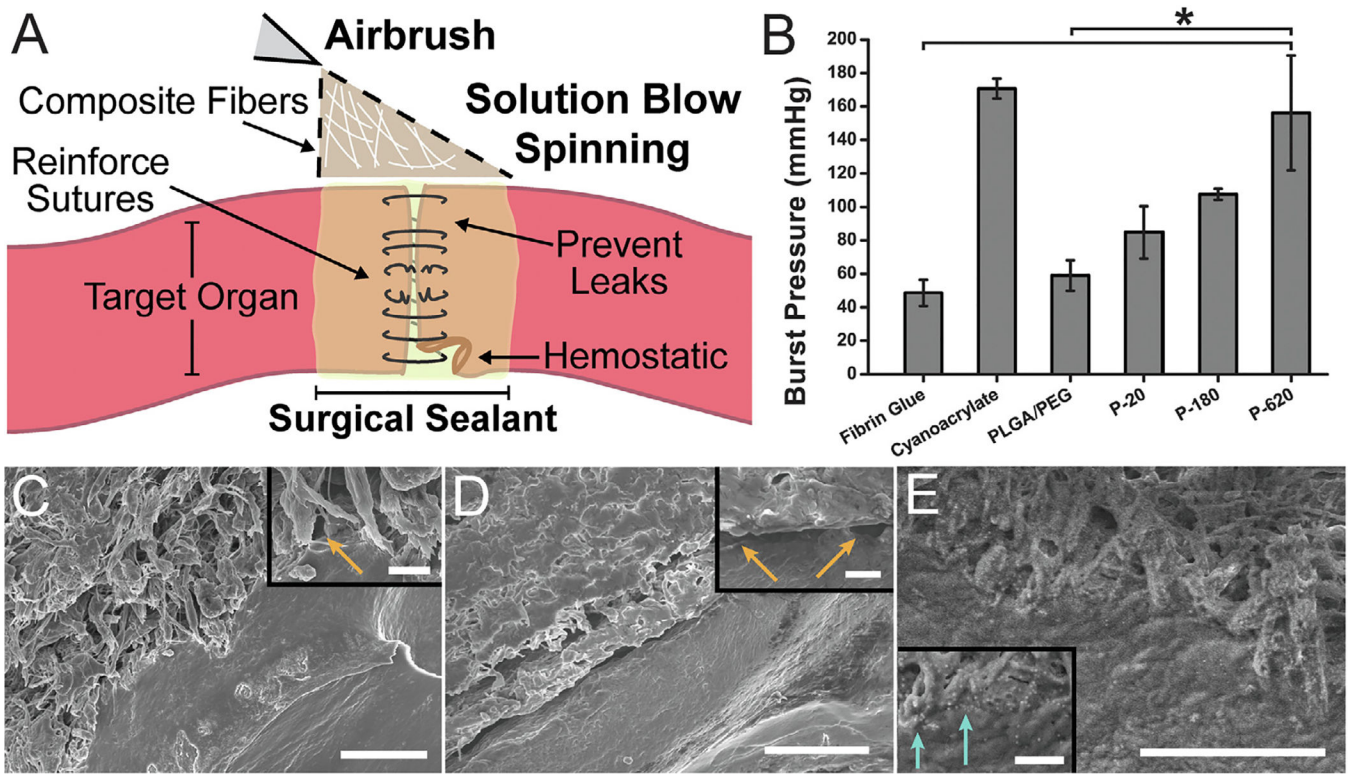

Fig. 2.

Performance of polymer-particle composite surgical sealants is enhanced by incorporating silica particles. (A) Schematic representation of direct deposition of polymer composite fibers onto a target organ. (B) Average burst pressures measured for different surgical sealants. Asterisk indicates statistically significant difference ($p < 0.01$) between the groups. Scanning electron microscope (SEM) images of intestinal tissue-sealant interface for (C) PLGA, (D) PLGA/PEG, and (E) P-620. Orange arrows indicate voids between the polymer and porcine intestinal tissue. Light blue arrows indicate silica particles at the interface between polymer and tissue. Scale bars = 50 mm for main image, 5 mm for inset. Composite surgical sealants are denoted “P-X”, where “X” is the diameter of the silica particles incorporated into PLGA/PEG. (For interpretation of the references to colour in this figure legend, the reader is referred to the web version of this article.)

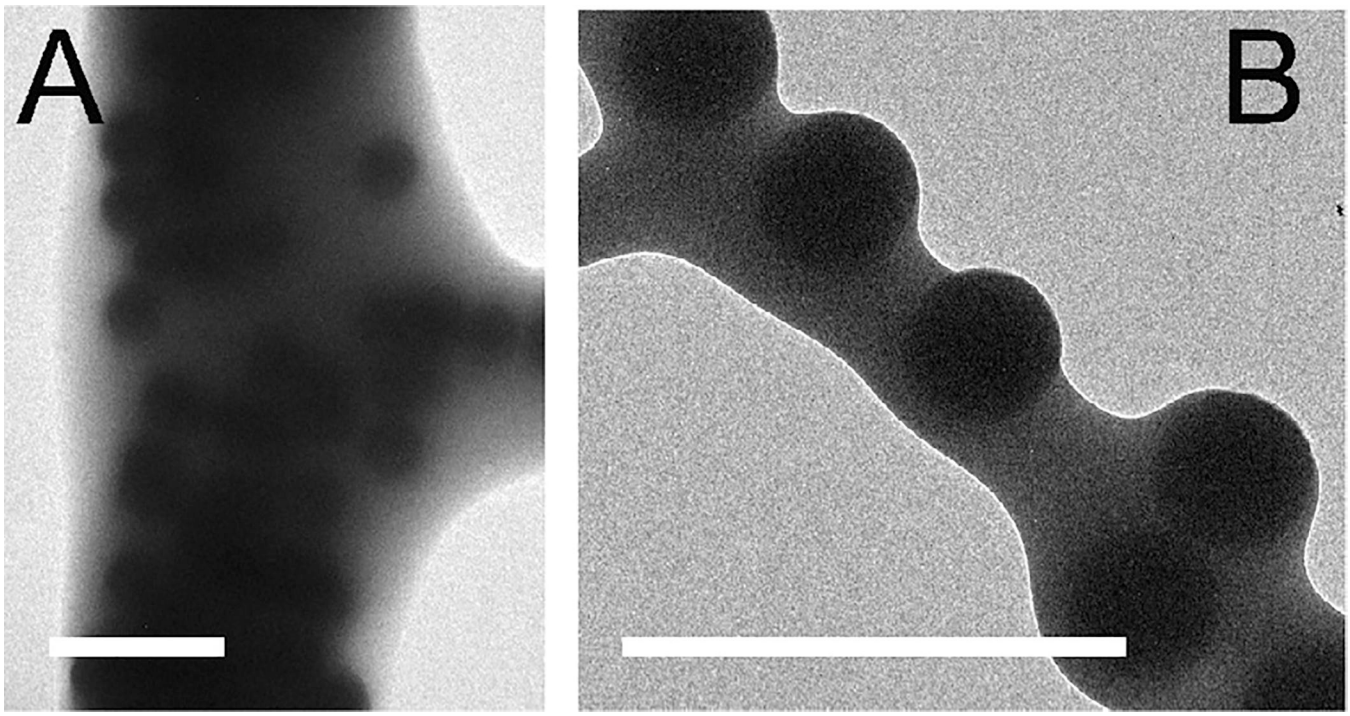

Fig. 3.

Silica particles are homogenously distributed throughout fibers produced by solution blow spinning. They are also present at the surface of fibers. Surface roughness is roughly proportional to particle diameter. (A–B) Transmission electron microscope (TEM) images of P-620 fibers. Scale bars = 2 μm.

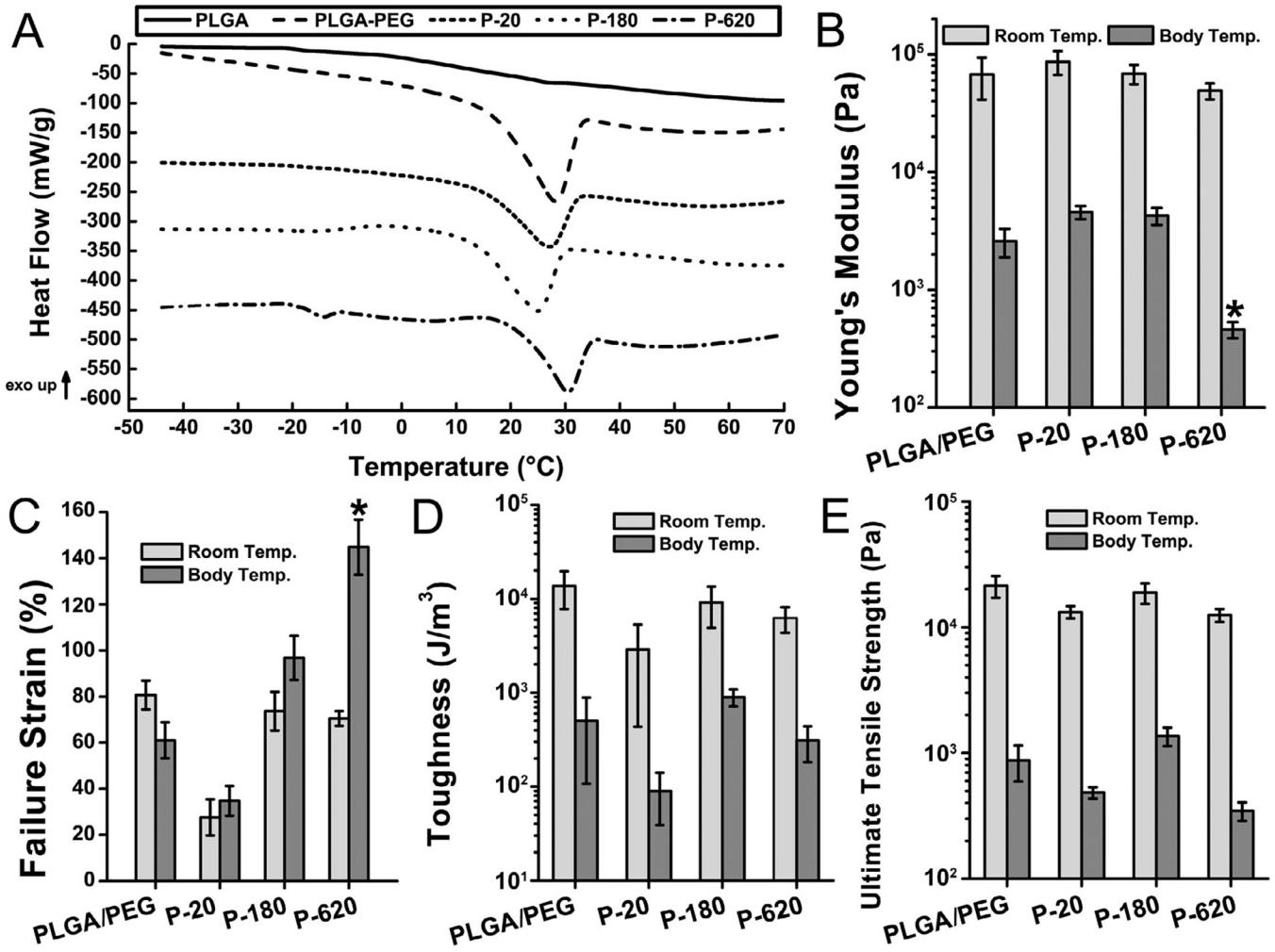

Fig. 4.

All polymer composites containing silica particles had body-temperature mediated thermal transitions, but mechanical properties varied depending on particle size. Composite sealants containing the largest particles tested (P-620) had reduced Young's modulus and increased failure strain, indicating improved flexibility and crack suppression. Asterisks indicate statistically significant differences ($p < 0.01$) between the indicated group and all other groups. (A) Modulated differential scanning calorimetry (MDSC) of sealants. Curves have been shifted vertically for clarity. (B) Young's modulus, (C) failure strain in tensile testing, (D) toughness, and (E) ultimate tensile strength in tensile testing at room temperature and body temperature (37 °C). Composite surgical sealants are denoted "P-X", where "X" is the diameter of the silica particles incorporated into PLGA/PEG.

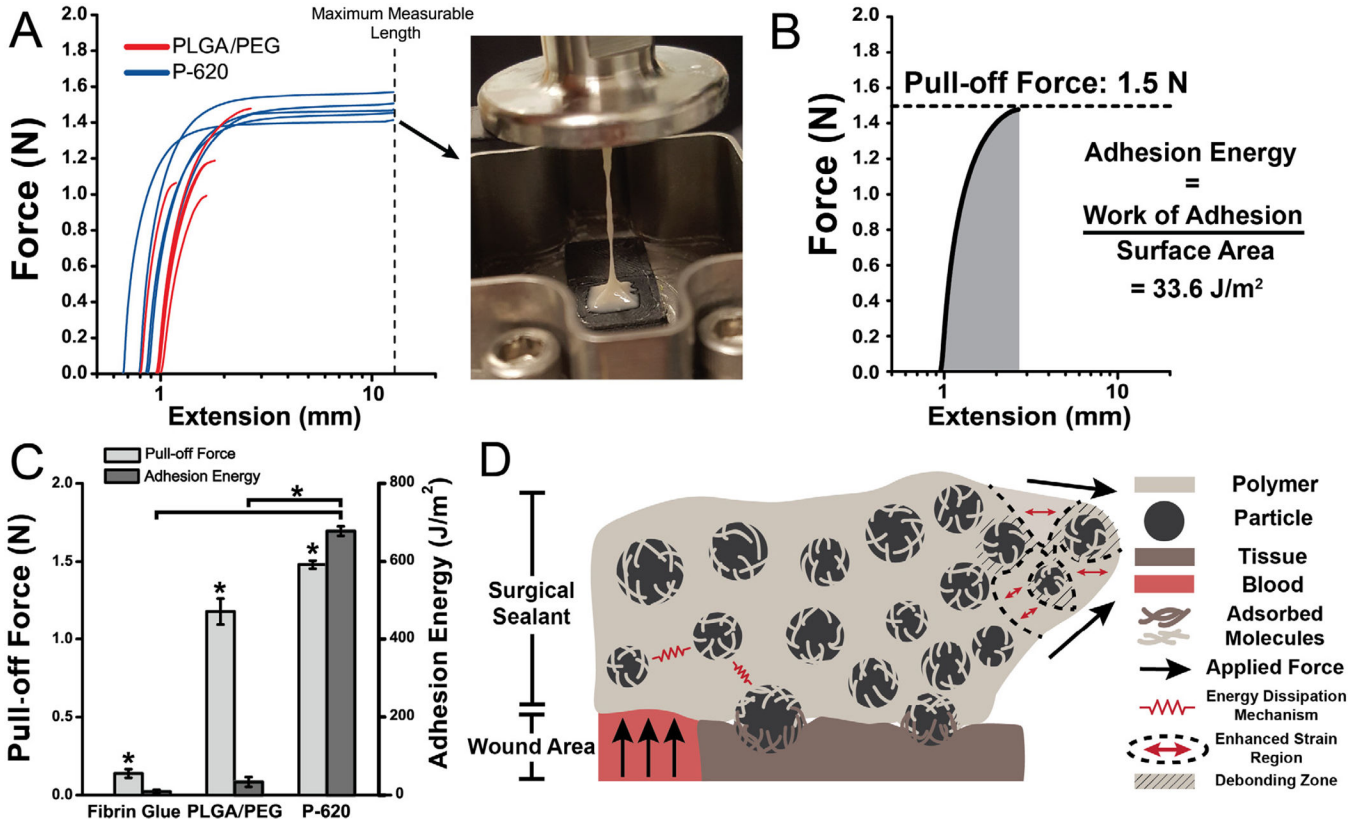

Fig. 5.

Composite sealants containing the largest particles tested (diameter of 620 nm) had increased adhesion force and energy compared to the non-composite control, PLGA/PEG. This was the result of adsorption of polymer chains to with particles at the interface and particle-composite toughening mechanisms. Asterisks indicate statistically significant ($p < 0.01$) differences. (A) Force-extension curves of pull-off adhesion testing. Inset: Image showing thread formation leading to cohesive failure of P- 620. (B) Sample curve analyzed for pull-off force (peak force measured) and adhesion energy (integral of force curve, normalized for surface area at interface). (C) Pull-off adhesion force and adhesion energy for PLGA/PEG and P-620. (D) Schematic illustrating the multiple toughening and adhesion enhancing mechanisms in particle-polymer composite sealants, including polymer chain adsorption to particles at the interface, suppressed crack propagation due to multiple regions of stress concentration, and energy dissipation as the reinforced sealant is deformed. Composite surgical sealants are denoted “P-X”, where “X” is the diameter of the silica particles incorporated into PLGA/PEG.

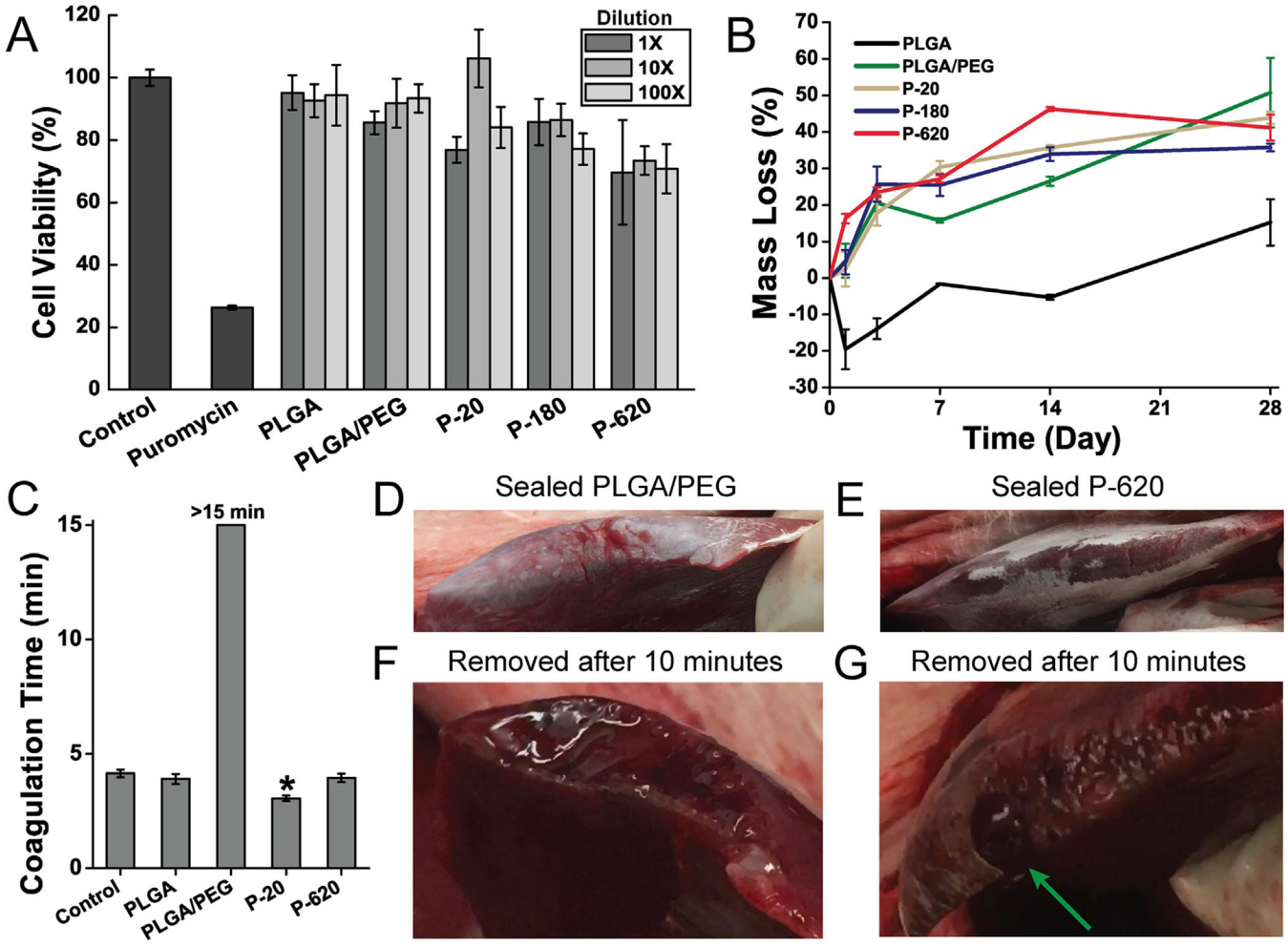

Fig. 6.

Polymer blend surgical sealants incorporating silica particles (denoted “P-X”, where “X” is the diameter of the silica particles incorporated into PLGA/PEG) have acceptable cell viability, appropriate degradation rate, and enhance hemostasis in vitro and in vivo. (A) Cell viability of L929 fibroblasts exposed to simulated in vitro 24 h extractions from various polymer-particle composite sealants. (B) Mass loss from fiber mats incubated at 37 °C in phosphate buffered saline (PBS). (C) Coagulation time measured by time to form a mechanically stable clot in an inverted vial. Asterisk indicates statistically significant difference between indicated group and all other groups. (D–G) *In vivo* comparison of hemostatic efficacy in a porcine liver laceration model. Immediately after resection, the liver surface was sprayed with polymer blend surgical sealant without silica particles (PLGA/PEG, D) and with 620 nm silica particles (P-620, E). (F) When PLGA/PEG was removed after 10 min, the resected area of the liver had not achieved hemostasis. (G) P-620 caused coagulation across the surface of the resection except for at a large hepatic vein, which is indicated by the green arrow. Composite surgical sealants are denoted “P-X”, where “X” is the diameter of the silica particles incorporated into PLGA/PEG. (For interpretation of the references to colour in this figure legend, the reader is referred to the web version of this article.)

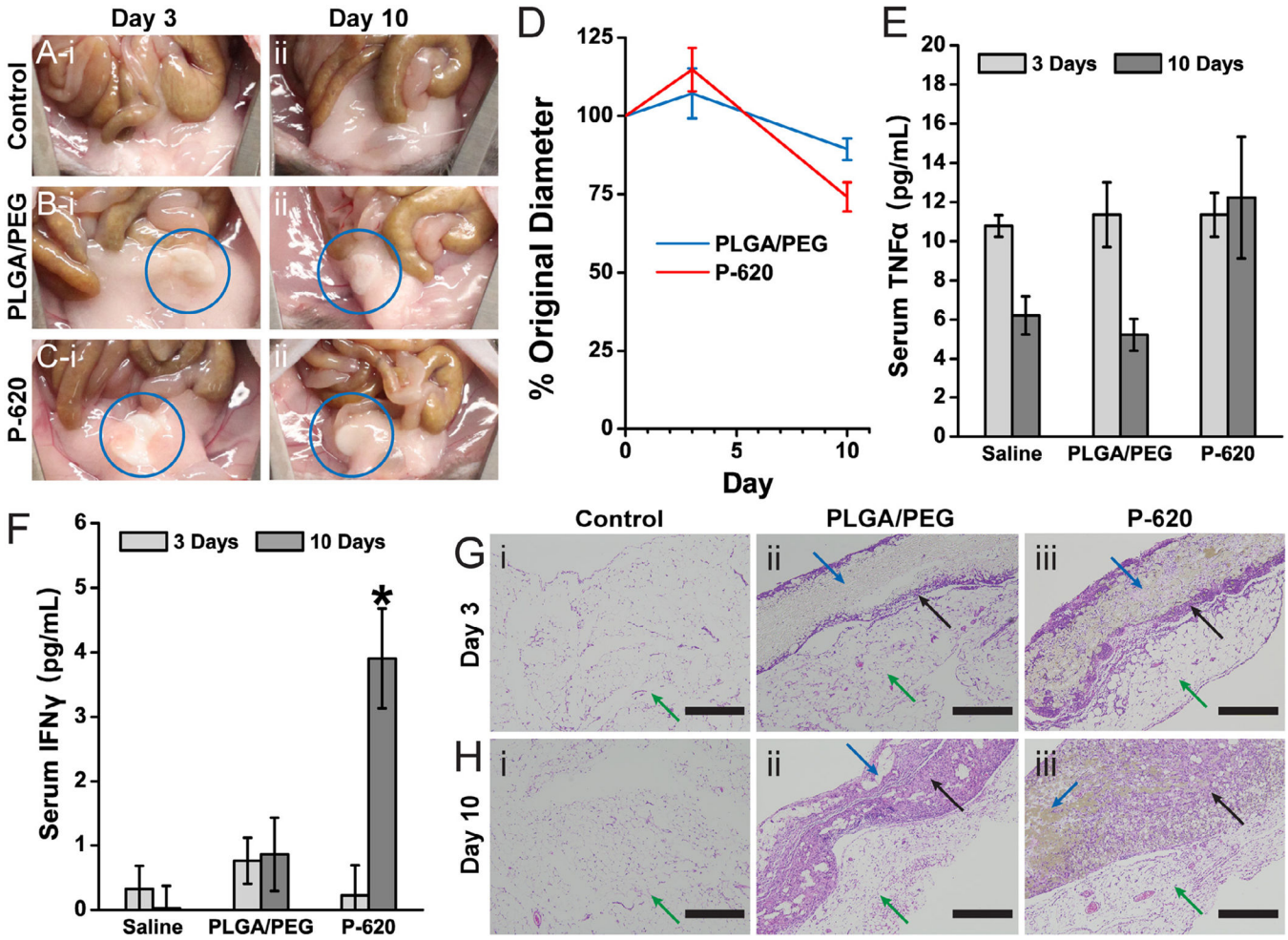

Fig. 7.

Polymer blend composite surgical sealants produces a mild inflammatory response. The composite sealant containing 620 nm silica particles (P-620) was tested against PLGA/PEG by intraperitoneal implantation. Pictures of the implant site showing minimal gross inflammation at 3 days (i) and 10 days (ii) for a control saline injection (A), PLGA/PEG (B), and P-620 (C). The implanted disks of surgical sealant were engulfed by the abdominal fat pads (blue circle). Both disks decrease in diameter over 10 days by approximately 25% (D). Serum concentrations of TNFα (E) and INFγ (F) are roughly equivalent, except for the increased concentration of 10-day INFc. Sections of the abdominal fat pads adjacent to the implantation site were stained with hematoxylin and eosin (G–H). Scale bars = 400 lm. Green arrows point to the abdominal fat pads, blue arrows point to the sealant disk, and black arrows point to areas of cellular infiltration into the surgical sealant disks. (For interpretation of the references to colour in this figure legend, the reader is referred to the web version of this article.)

Table 1

Composition of spinning solutions for tested polymer blend surgical sealants incorporating silica particles.

Name	% PLGA [w/v]	% PEG [w/v]	% Particle [w/v]	Particle Diameter [nm]	Particle Zeta Potential [mV]	Particle Type
PLGA/PEG	10	5	0	N/A	N/A	N/A
P-20	10	5	5	19 ± 2[a]	−37 ± 2[a]	Silica nanopowder
P-180	10	5	5	181 ± 2	−43.9 ± 0.2	Stöber silica
P-620	10	5	5	619±8	−41.9±0.2	Stöber silica

[a]Characterized previously [26].

Table 2

Weight fractions (w), volume fractions (φ), and estimated specific surface area of particles (calculated using particle diameter from Table 1) for solid composite sealants incorporating silica particles.

Solid Sealant	w_{plga}	w_{peg}	$w_{particle}$	ϕ_{plga}	ϕ_{peg}	$\phi_{particle}$	Specific Surface Area [m^2/g]
PLGA/PEG	0.67	0.33	0	0.64	0.36	0	N/A
P-20	0.50	0.25	0.25	0.54	0.30	0.16	143.0
P-180	0.50	0.25	0.25	0.54	0.30	0.16	15.1
P-620	0.50	0.25	0.25	0.54	0.30	0.16	4.4